Applied Physics Letters

Green ultra-wideband antenna utilizing Mie resonances in cactus

Cite as: Appl. Phys. Lett. **120**, 053301 (2022); https://doi.org/10.1063/5.0077338
Submitted: 01 November 2021 • Accepted: 06 January 2022 • Published Online: 31 January 2022

Abhinav Jain, Dmytro Vovchuk, Roman E. Noskov, et al.

Applied Physics Letters ARTICLE scitation.org/journal/apl

Green ultra-wideband antenna utilizing Mie resonances in cactus

Cite as: Appl. Phys. Lett. **120**, 053301 (2022); doi: 10.1063/5.0077338
Submitted: 1 November 2021 · Accepted: 6 January 2022 ·
Published Online: 31 January 2022

Abhinav Jain,[1,a)] Dmytro Vovchuk,[1] Roman E. Noskov,[1] Eran Socher,[1] and Pavel Ginzburg[1,2]

AFFILIATIONS

[1]School of Electrical Engineering, Tel Aviv University, Tel Aviv 69978, Israel
[2]Center for Photonics and 2D Materials, Moscow Institute of Physics and Technology, Dolgoprudny 141700, Russia

[a)]Author to whom correspondence should be addressed: abhinavjain@mail.tau.ac.il

ABSTRACT

While plants are typically supposed to restrict the performance of radio frequency transceiver systems, they can act as efficient biogenic elements of control. A high fraction of water inside vegetation gives rise to multiple electromagnetic Mie resonances, originating from interplaying a naturally high permittivity and a form factor. Opuntia ficus-indica, known as nopal cactus, is a representative example whose succulent stems or cladodes contain nearly 75–85% water. Here, we present an Opuntia-based broadband omnidirectional antenna element, operating at several Wi-Fi communication bands, spanning from 900 MHz to 7.7 GHz. A high relative permittivity in the GHz range exceeds 20. As a result, a variety of Mie resonances within the cladode are measured and revealed by the multipole expansion technique. Modal hierarchy, resonantly excited with a coaxial cable, is demonstrated to provide a broadband impedance matching below −10 dB over the ∼150% bandwidth. Further investigations of plants as functional electromagnetic elements can contribute to the general trend of environment friendly multifunctional devices, promoting development of green technologies.

A variety of microwave based applications, involving green vegetation components (e.g., stems, branches, leaves, and fruit), play an important role in industrial, scientific, and medical sectors.[1] Contactless noninvasive electromagnetic approaches, widely used in medical diagnostics, can be applied for agricultural needs. Penetration of electromagnetic waves into a medium depends on a material attenuation coefficient at a chosen spectral range. Lower frequencies typically have better penetration capabilities with a penalty of a reduced spatial resolution. In general, goods quality monitoring, tracking, and managing agriculture activities are made possible by mapping an averaged dielectric permittivity on parameters of interest, including moisture, ionic concentration, and material density.[2] Quite a few crops, including their quality and biological activities, were assessed with the aid of remote electromagnetic sensing.[3–7]

Many permittivity retrieval techniques were developed for testing agricultural products. While low frequency parameters are typically assessed with capacitive approaches,[8] retrieval of MHz–GHz permittivity demands using alternative methods.[2] However, open ended coaxial technique is used for the most for assessing liquids and semi solid materials above 100 MHz.[5,9–12] Electromagnetic properties of potato,[11] tomato,[4] pear,[12] banana,[11,12] orange,[11] apple,[11–13] carrot,[10–12] and banana leaves[14] were investigated at X-band (8.0–12.0 GHz) and taken toward the remote monitoring of their growth.[15,16] Additional reports investigated absorber materials based on fibrous plants,[17,18] while few others focused on determining the impact of vegetation on microwave propagation.[4,19]

Another area, where electromagnetic properties of plants play an important role, is wireless communications, where crops introduce a significant attenuation factor, contributing to the free space propagation. While in a vast majority of cases, vegetation is considered as a limiting factor, reducing channel capacities,[20,21] they can also be used as elements of control. Having high concertation of water, worldwide available plants can be utilized as dielectric resonant antenna (DRA) elements.[22,23] In particular, cactuses are good candidates for testing the concept.

Opuntia ficus-indica, or eastern prickle pear or green cladode, belongs to the cactus family Cactaceae. *O. ficus-indica* is a Crassulacean acid metabolism (CAM) plant, which can store a large amount of water in its leaves or cladodes. *O. ficus-indica* cladodes are used as vegetable in South and Central America and in various parts of the world. This crop, containing nicotiflorin, can provide an effective treatment against many diseases.[24] Furthermore, cactuses are widespread throughout arid, semiarid regions of drought and desert areas where communication is a very challenging task. Cladodes, consisting of 75%–85% water,[25] can possess multiple Mie resonances and act as natural DRAs. Dielectric properties of constitutive materials[26]

along with a geometrical shape of a scatterer govern its interaction with electromagnetic waves. Here, we investigate *O. ficus-indica* capabilities to serve as an efficient antenna device, which might be customized and contribute to several WLAN applications and Wi-MAX covering all frequency bands. In particular, 900 MHz, 2.4, 3.6, 4.9, 5, 5.9, and 6 GHz are used for Wi-Fi communication, which is under the IEEE 802.11 protocol.[27–29]

Here, we show that the modal hierarchy, resonantly excited with a standard coaxial cable, is responsible to provide a broadband impedance matching bandwidth of approximately 150% for $S_{11} < -10$ dB from 900 MHz to 7.7 GHz frequency band with next to omnidirectional directivity patterns and close to 0 dB gain. The manuscript is organized as follows: the electromagnetic properties of the *O. ficus-indica* are discussed first and after identifying the range of frequencies a broadband antenna performance is demonstrated. Then, the scattering and multipole decomposition analysis of the standalone plant is presented followed by the conclusion. In order to untie the broadband antenna performance from a specific crop under investigation, parametric studies over possible cladode dimensions are performed and come under the supplementary material part.

In order to perform numerical analysis of electromagnetic interactions with the plant, material parameters of the latter should be retired. While there are quite a few techniques in the field,[30–33] open ended coaxial probe method was proven to be an efficient tool to determine the dielectric properties of the fruits and vegetables over a wide frequency range.[32,33] Poking a probe into a plant allows performing a local retrieval of electromagnetic properties. Cactus consists of a small fraction of carbs, magnesium, potassium and, primarily, of 75%–85% water, making the object to be high-epsilon in the GHz spectral range. The plant's permittivity is influenced by the ionic conductivity and the bound water relaxation. Since the amount of water may vary in different positions along the cladode, there is a reason to keep the structure unperturbed in order to account for possible structural and position dependence of the permittivity along the cladode. The dispersion characteristics of the *O. ficus-indica* (eastern prickly pear) have been measured with the fresh and one-day-old sample in

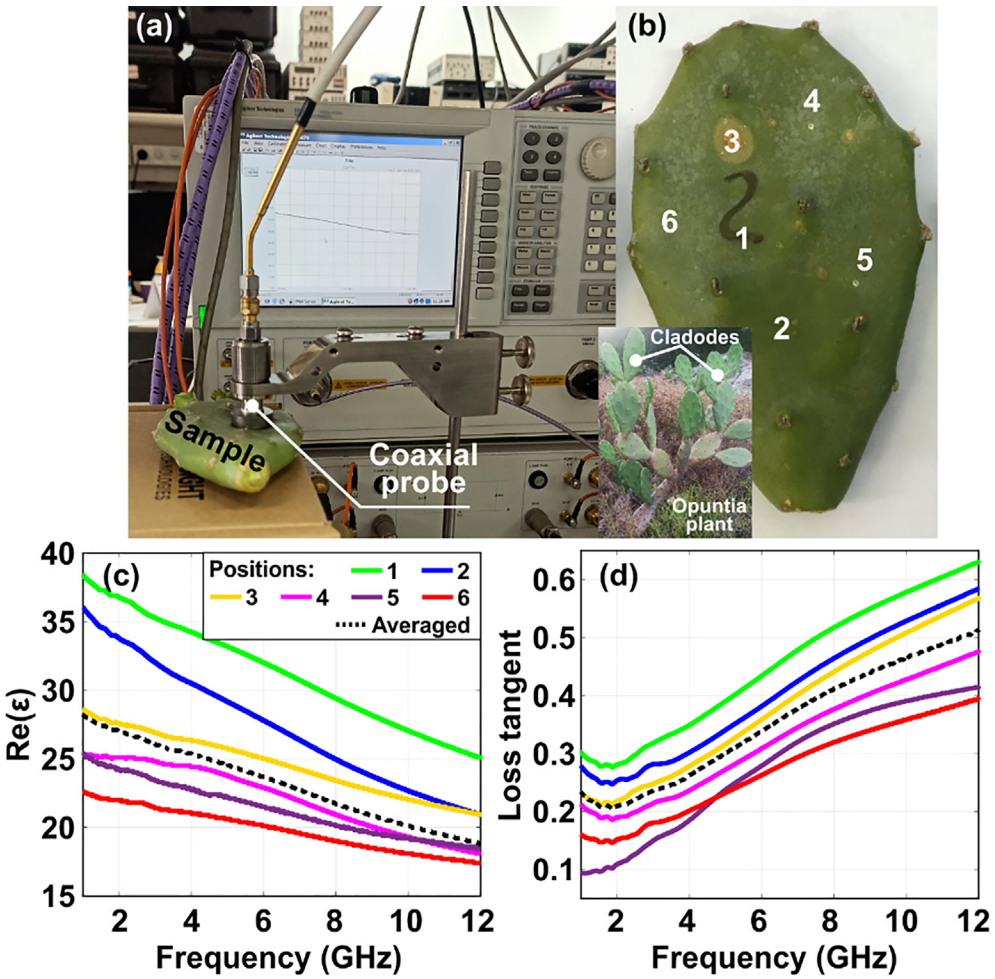

FIG. 1. *O. ficus-indica* permittivity retrieval. (a) Photograph of the setup—the open-end coaxial probe method. (b) Photograph of the cladode. Points, where the probe poked the sample, are indicated with the numbers 1–6. (c) Real part of the permittivity [Re(ε)] and (d) loss tangent at six positions along the cladode as a function of frequency. The dashed lines—averaged values.

the frequency range of 1–12 GHz, as shown in Fig. 1(a). The measurement is performed with a vector network analyzer (VNA, Keysight N1501A), a coaxial probe and software post processing. The system was calibrated using air, short and de-ionized water (25 °C) prior to the main experiment. The data were acquired for different positions on the *O. ficus-indica* sample numbered as 1–6, shown in Fig. 1(b). The real part of the permittivity (Re (ε)) and the loss tangent, obtained at six probe positions as a function of frequency, appear in Figs. 1(c) and 1(d), respectively. The results are the same for both samples. The averaged value is represented with the dashed line. While the results at the probing points differ from each other by almost 20%–30%, they all share the same dispersion behavior. It is quite remarkable that the permittivity has a negative slope with the frequency increase. In fact, similar phenomenon has been observed in several natural forms[30,32] and is attributed to the ionic conductivity and the bound water relaxation. It can be seen that the permittivity drops with approaching the cladode's margin, verifying the fact that the water content is maximal at the center, where the structure is wider. The overall values of the permittivity are quite high, being accompanied by moderate losses that allow considering the plant as a DRA[22,23] or a scatterer. Since the dielectric constant has a strong temperature dependence owing to the presence of water, all the experiments were obtained at nearly the same environmental conditions.

Next, we consider the *O. ficus-indica* antenna performance. The cladode is excited by a monopole above a ground plane (1.5 mm FR4 with 0.035 mm thick copper layer), pinched into the bottom of the structure [Fig. 2(a)]. The wire length (L) is L = 18.5 mm (quarter wavelength ($\lambda/4$) at ~4 GHz), and the wire radius (r) is approximately $r < \lambda/20$, where r = 0.75 mm, fixed with respect to the 50 Ω SMA connector. Figure 2(b) shows the reflection coefficient (S_{11} in dB) as a function of frequency for numerical simulations (see details below) and measurements, which are in a reasonable agreement. Without the cladode, a single resonance around 4 GHz, corresponding to a dipole eigenmodes of the wire, is observed. Numerical and experimental results for the cladode are shown in Fig. 2(b), demonstrating the bandwidth ranging from 900 MHz to 7.7 GHz, which can be considered as an ultra-wideband (~150% for $S_{11} < -10$ dB). Three different resonances are obtained at 1.26, 2.46, and 4 GHz for the simulations and 1.2, 2.3, and 3.5 GHz for the experiment. The experimental results have minor deviations from the numerical prediction and are attributed to variations in original material properties. It is quite remarkable that the position of the poking monopole within the cladode has only a minor impact on S_{11}, which is very beneficial taking into account a natural diversity of cladodes, which will be addressed in the supplementary material section.

Figure 2(c) shows the comparison of gain patterns obtained numerically and experimentally in the anechoic chamber. The patterns are demonstrated for different frequencies, i.e., 1.26, 2.46, 4, and 6 GHz numerically and 1.2, 2.3, 3.5, and 6 GHz at experiments. Dipolar-like patterns with Omni-directional in-plane coverage are observed. Table I summarizes directivities and gains at the representative frequencies. Losses start to affect the performance at shorter wavelengths, as it can be predicted by observing dispersions in Fig. 1.

In order to link the broadband performance of the cladode antenna with the Mie resonances hierarchy, the scattering performance of the standalone plant will be performed next. To analyze scattering efficiency of the *O. ficus-indica* theoretically, we consider the cladode as a homogeneous two-axial prolate ellipsoid with the spatially averaged permittivity and loss tangent, shown in Fig. 1. The semi-major axis of 55 mm, the minor axis of 34 mm, and the thickness of 16 mm were chosen, based on the sample geometry shown in Fig. 1(b). Full-wave numerical analysis was performed with a 3D finite element method (FEM) using CST Microwave Studio. Figure 3 shows the spectra of the scattering efficiency (the scattering cross section

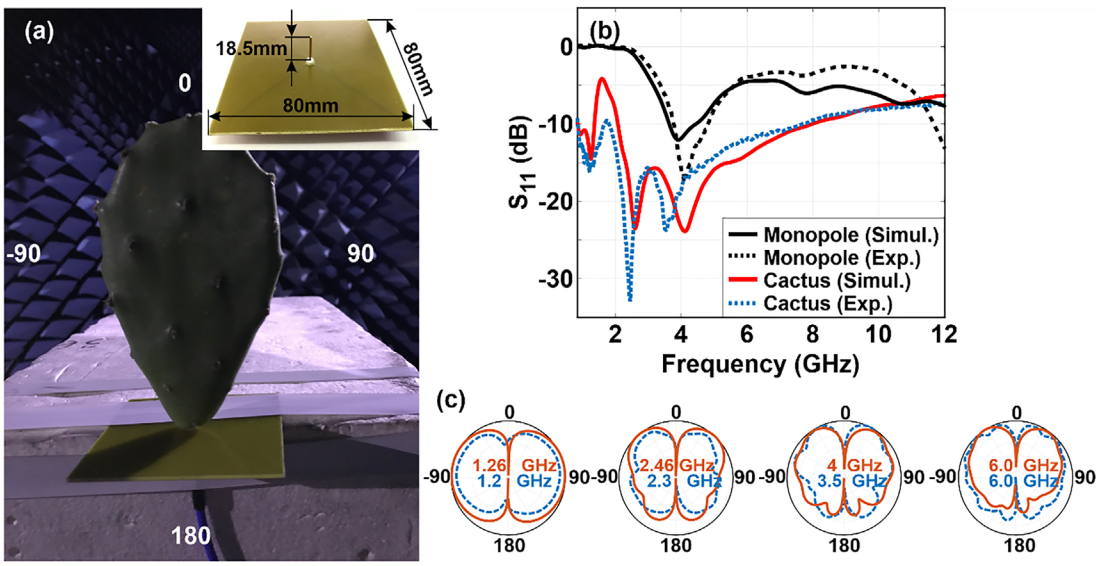

FIG. 2. (a) Cladode antenna in an anechoic chamber. The cladode is poked with a monopole feed. Inset—the monopole above FR4 substrate. (b) S_{11} in dB as a function of frequency. Black solid line—standalone monopole, simulation; black dashed line—standalone monopole, experiment; red solid line—cactus antenna, simulation; blue dashed line—cactus antenna, experiment. (c) Gain patterns in the plane, containing the broader projection of the cladode. Frequencies are indicated in the plots. Orange solid lines—simulation; blue dashed lines—experiment.

TABLE I. Directivity (D) and gain (G) at several frequencies: simulations and experimental measurements.

Simulations			Experiment		
f (GHz)	D (dBi)	G (dBi)	f (GHz)	D (dBi)	G (dBi)
1.2	1.91	1.07	1.2	2.37	−0.07
1.26	2.03	0.817	1.3	2.81	−1.08
2.4	6.13	1.79	2.4	3.24	−1.3
3.6	5.16	−0.844	3.5	3.83	−0.68
4	4.52	−1.4	4	4.05	−2.31
6.0	3.96	−2.83	5.2	3.39	−3.93
7.9	2.21	−5	7.7	3	−4.54

normalized by the object geometric cross section within the plane wave front) for a plane wave polarized along x-($k_x = k_z = 0, k_y = k_0$), y-($k_x = k_y = 0, k_z = k_0,$), and z-axes ($k_x = k_z = 0, k_y = k_0$) (ellipsoid major axes).

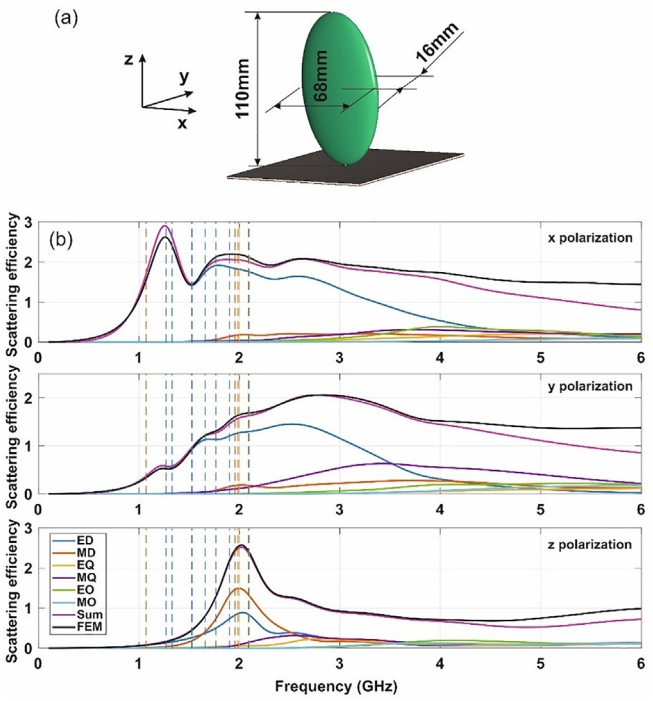

FIG. 3. (a) Spatial dimensions of the cladode used in simulations. (b) Scattering efficiency of a cladode and its multipole expansion for various polarizations of the plane wave along the ellipsoid major axis. Vertical dashed lines denote the frequencies of the lowest order eigenmodes. Blue, red, and yellow lines correspond to the eigenmodes with dominating ED, MD, and EQ contributions, respectively. Contribution of each multipole is marked with different colors: blue, electric dipole (ED); red, magnetic dipole (MD); yellow, electric quadrupole (EQ); violet magnetic quadrupole (MQ); green, electric octupole (EO); and sky blue, magnetic octupole (MO), respectively. The sum of multipole contributions is denoted with purple (Sum), and the scattering efficiency obtained by the straightforward integration of the Poynting vectors is marked with black (FEM).

To provide insights into the system scattering behavior, we employ a Cartesian multipole expansion method, which allows us to present the scattering cross section up to the terms of the third order included as follows:[34]

$$\sigma_{\text{scat}} = \frac{k^4}{6\pi\varepsilon_0^2|\mathbf{E}_0|^2}|p_j|^2 + \frac{k^4\varepsilon_h}{6\pi\varepsilon_0^2c^2|\mathbf{E}_0|^2}|m_j|^2 + \frac{k^6\varepsilon_h}{80\pi\varepsilon_0^2|\mathbf{E}_0|^2}\left|Q_{jk}^{(e)}\right|^2 + \frac{k^6\varepsilon_h^2}{80\pi\varepsilon_0^2c^2|\mathbf{E}_0|^2}\left|Q_{jk}^{(m)}\right|^2 + \frac{k^8\varepsilon_h^2}{1890\pi\varepsilon_0^2|\mathbf{E}_0|^2}\left|O_{jkl}^{(e)}\right|^2 + \frac{k^8\varepsilon_h^3}{1890\pi\varepsilon_0^2c^2|\mathbf{E}_0|^2}\left|O_{jkl}^{(m)}\right|^2, \quad (1)$$

where Einstein's summation notation is used, k is the vacuum wave number, $|\mathbf{E}_0|$ is the amplitude of the incident field, ε_h is the permittivity of the host media, ε_0 is the permittivity of vacuum, p_j and m_j are the basic electric dipole (ED) and magnetic dipole (MD) moments, $Q_{jk}^{(e)}$ and $Q_{jk}^{(m)}$ are the basic electric and magnetic quadrupoles (EQ and MQ), and $O_{jkl}^{(e)}$ and $O_{jkl}^{(m)}$ are basic electric and magnetic octupole (EO and MO). The exact expressions for them can be found in Refs. 16 and 34. The accuracy of this expansion is assessed vs the comparison with the scattering efficiency obtained by straightforward integration of the Pointing vector, denoted as FEM in Fig. 3. An excellent agreement between FEM and the sum of multipole contributions is observed up to 4 GHz. The slight disagreement for higher frequencies is caused by appearance of the multipoles beyond the third order. The multipole expansion shows that for x- and y-polarized plane waves, ED provides a dominant contribution to all resonances observed in the scattering efficiency in a wideband domain from 1 to 3 GHz. For a z-polarized wave, both MD and ED contribute to the scattering for the resonance at 2 GHz.

TABLE II. Characterization of the cladode eigenmodes: eigen frequencies, mode type in accord to the Cartesian coordinates, dominating multipoles, Q factors for lossless and lossy cases.

Eigen frequency (GHz)	Mode type	Contributing multipoles	Q factor (lossless)	Q factor (lossy)
1.068	TM_{111}	MD (M_z − mode)	14.8	3.5
1.269	TM_{211}	ED+MQ (P_y − mode)	27.6	4.1
1.33	TM_{121}	ED (P_x − mode)	2.8	2.5
1.524	TM_{141}	MD+EQ+MO	6.3	4.3
1.5285	TM_{311}	MD+MO	66.6	2.6
1.66	TM_{221}	ED+MQ	109.1	4.7
1.766	TM_{431}	ED+MQ	31.5	3.8
1.899	TM_{331}	MD+EQ	26.5	4
1.9	TM_{321}	ED+MQ+EO	93.8	4.3
1.955	TM_{111}	MD (M_x − mode)	12	3.5
1.987	TM_{111}	MD (M_y − mode)	11.3	3.4
2	TM_{511}	MD+EQ+MO	69.5	4.2
2.09	TM_{221}	ED+MQ (P_z − mode)	25.7	4
2.095	TM_{431}	ED+MQ+EO	53.5	4.4
2.1	TM_{421}	EQ	62.2	4.2
2.21	TE_{221}	MQ	49.1	4.4

To elucidate this behavior, we perform eigen mode analysis of the cladode and distinguish relative multipole contributions to the eigenmodes. The eigen frequencies along with contributing multipoles and mode type and profile are summarized in Table II and Fig. 4. Vertical dashed lines in Fig. 3 denote the frequencies of the lowest order eigenmodes. The maximum at 1.26 GHz (which appears in experiment at 1.2 GHz) corresponds to ED-type TM_{211} and TM_{121} eigenmodes with ED oriented along y- and x-axes. The broad maxima localized between 1.5 and 2.2 GHz, observed in experiment around 2.3 GHz, is caused by superposition of TM_{221}, TM_{431}, TM_{331}, TM_{321}, TM_{511}, TM_{221}, TM_{431}, and two TM_{111} eigenmodes. All these modes are governed by ED and MD (Fig. 4), which manifest in the experiment as dipole-like radiation patterns, shown in Fig. 2(c). The absence of narrow peaks in the scattering corresponding to individual

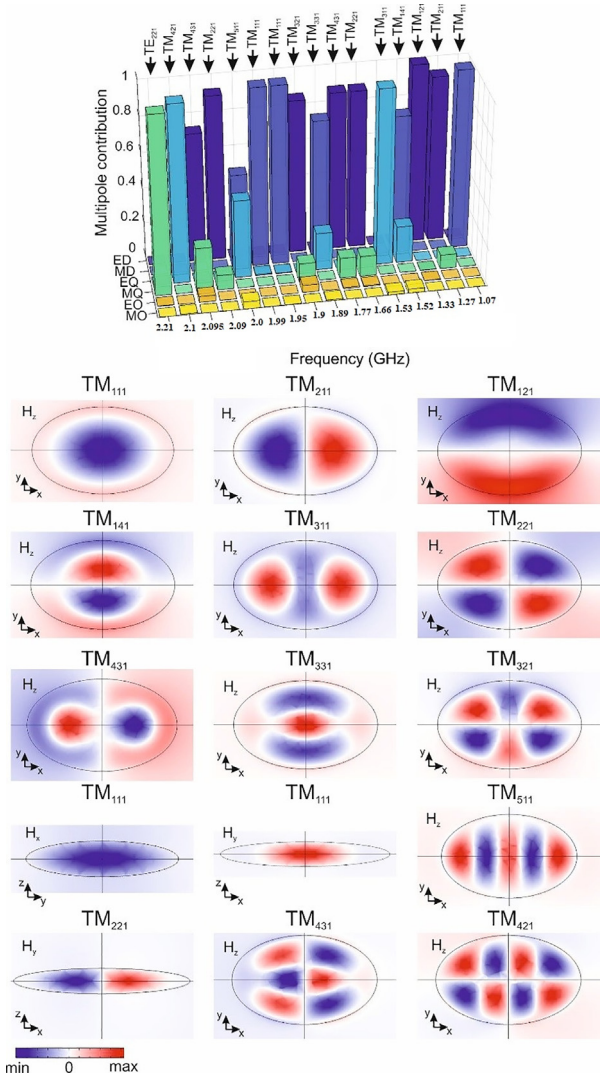

FIG. 4. Multipole contributions to the cladode's eigenmodes: type of eigenmodes is presented according to the Cartesian coordinate system. Profiles of the eigenmodes providing dominant contributions to the resonances observed in the scattering cross section in Fig. 3.

eigenmodes can be attributed to internal losses of the cactus, which drops the Q factor of eigenmodes from ∼10–100 to ∼3–5 (Table II). Considering losses of the cladode, we get a wide bandwidth and reasonable quality factors in the broad frequency range, relevant to broadband wireless communications.

O. ficus-indica or its succulent stems called cladodes were demonstrated to serve as an efficient dielectric resonant antenna. Owing to its high water contain with dissolved natural minerals, the structure supports a variety of resonant modes, which overlap in frequency with each other. This resonance cascading allows covering a rather broad frequency range, as it is clearly seen in electromagnetic scattering spectrum. Coherent excitation of the modes allowed demonstrating broadband impedance matching to an initially non-resonant monopole, realized as a short wire above a ground plane. As a result, 150% bandwidth (−10 dB level) was experimentally demonstrated, covering the frequency range between 900 MHz and 7.7 GHz. Substantial efforts are performed nowadays toward investigating green environmentally friendly technologies. In many cases, those endeavors come with an expense of performance degradation, putting ecological aspects at the cornerstone. Taking a green communication approach, being cheap and effective at the same time, can provide an additional boost to this emerging and highly important field.

See the supplementary material for bandwidth robustness to cladode's variability: *O. ficus-indica* plants naturally have different sizes and shapes, which might affect antenna characteristics. While the performances do depend on the cladode's shape, the poking monopole can serve as an essential degree of freedom, capable to tune the device toward a broadband operation. The eastern prickly pear belongs to one of the species in Opuntia ficus-indica from total of 1800 species in cactus family. The cladode or pads of eastern prickly pear plant are generally not very large, and these can be of 5–17 cm (50–170 mm) long and 4–12 cm (40–120 mm) wide. In order to verify a certain level of robustness to the size variations, we investigate S_{11} as a function of (i) monopole length and (ii) variations in width, height, and thickness of the cladode. Since this parametric space cannot be presented on a single three-dimensional plot, a single parameter is varied each time. The cladode geometrical parameters are taken as width 68 mm, height 110 mm, and thickness of 16 mm. Figure S1(a) shows the color map of S_{11} as a function of frequency (1–12 GHz), and the monopole length varies from 10 to 60 mm. Monopole resonance is the function of a change in monopole length. Figure S2 compares the bandwidth at the monopole resonance of 1.5, 4, and 6.5 GHz, where the bandwidth is maximum at the monopole resonance of 4 GHz (around 18.5 mm monopole length). Bandwidth at higher end remains almost same, whereas the resonance shifted to higher frequency with the increase in length as shown in Fig. S1(a). Figure S1(b) investigates the same parameter, taking the cladode thickness as a variable (10—2 mm). Reducing the thickness does not affect the resonance, however, leading to the bandwidth increase. Figure S1(c) shows the investigation with the changing the cladode's width from 40 to 120 mm. Here, the bandwidth and the resonance almost remain the same for the entire variation. Figure S1(d) demonstrates the behavior as a function the height from 50 to 170 mm. Here, the resonance remains the same but the bandwidth slightly improves as the height increases. These estimations of resonance and bandwidth characteristics support the claim that a variety of cladodes can serve as efficient antenna devices. We have also

investigated the performance in terms of gain and directivity with single and four cladode configuration similar to the cactus plant. Both directivity and gain have very little effect at lower frequencies and will remain almost same for the higher frequencies. Comparison of characteristics at different frequencies for single and four cladode configurations is presented in Table S1 in the supplementary material.

The authors acknowledge Avigdor Jacov Drucker for assisting with the parametric retrieval and Dr. Sergei Kosulnikov for discussion. P.G. acknowledges Russian Science Foundation under Project No. 20-19-00480 for supporting the data analysis part of the work. The research was supported by ERC StG "In Motion" (No. 802279) and PAZY Foundation (No. 01021248). This work was supported in part by the Ministry of Science and Higher Education of the Russian Federation (No. FSMG-2021-0005).

AUTHOR DECLARATIONS

Conflict of Interest

The authors declare that they have no competing interests.

Author Contributions

A.J., D.V., and R.E.N. contributed equally to this work.

DATA AVAILABILITY

The data that support the findings of this study are available from the corresponding author upon reasonable request.

REFERENCES

[1]B. L. Shrestha, "Microwave measurement and modeling of the dielectric properties of vegetation," Ph.D. dissertation (The University of Saskatchewan, Saskatchewan, Canada, 2006).
[2]S. Metlek, K. Kayaalp, I. B. Basyigit, A. Genc, and H. Dogan, Int. J. RF Microwave Comput. Eng. **31**, e22496 (2021).
[3]U. Pliquett, Food Eng. Rev. **2**, 74 (2010).
[4]T. Van Emmerik, S. Steele-Dunne, J. Judge, and N. Van De Giesen, in IEEE International Geoscience and Remote Sensing (2015), Vol. 275.
[5]S. O. Nelson, IEEE Trans. Dielectr. Electr. Insul. **13**, 688 (2006).
[6]R. Zywica, G. Pierzynowska-Korniak, and J. Wójcik, J. Food Eng. **67**, 413 (2005).
[7]A. B. Itolikar and M. L. Kurtadikar, J. Microwaves, Optoelectron. Electromagn. Appl. **16**, 954 (2017).
[8]D. E. Khaled, N. Novas, J. A. Gazquez, R. M. Garcia, and F. Manzano-Agugliaro, Sensors **15**, 15363 (2015).
[9]Z. Zhu and W. Guo, Sci. Rep. **7**(1), 71 (2017).
[10]V. N. Tran, S. S. Stuchly, and A. Kraszewski, J. Microwave Power **19**, 251 (1984).
[11]S. O. Nelson, Trans. ASAE **46**, 567 (2003).
[12]O. Sipahioglu and S. A. Barringer, J. Food Sci **68**, 234 (2003).
[13]W. chuan Guo, S. O. Nelson, S. Trabelsi, and S. J. Kays, J. Food Eng. **83**, 562 (2007).
[14]N. A. Zulkifli, W. F. Hoon, S. Z. Ibrahim, M. N. M. Warip, L. Y. Seng, and Y. B. Seok, in IEEE Student Conference on Research and Development (SCOReD) 2017: Inspiring Technology for Humanity: Proceedings (2018).
[15]A. Genc, I. B. Basyigit, H. Dogan, and B. Colak, J. Electromagn. Waves Appl. **35**(14), 1909–1921 (2021).
[16]P. D. Terekhov, A. B. Evlyukhin, D. Redka, V. S. Volkov, A. S. Shalin, and A. Karabchevsky, Laser Photonics Rev. **14**, 1900331 (2020).
[17]B. Colak, Microwave Opt. Technol. Lett. **61**, 2591 (2019).
[18]E. Jayamani, S. Hamdan, P. Ezhumalai, and M. K. Bakri, J. Teknol. **78**, 97 (2016).
[19]S. C. Steele-Dunne, J. Friesen, and N. Van De Giesen, IEEE Trans. Geosci. Remote Sens. **50**, 2618–2629 (2012).
[20]M. Paul, T. J. Bouma, and C. L. Amos, Mar. Ecol.: Prog. Ser. **444**, 31 (2012).
[21]A. A. Chukhlantsev, J. Electromagn. Waves Appl. **6**, 1043 (1992).
[22]S. Keyrouz and D. Caratelli, Int. J. Antennas Propag. **2016**, 6075680.
[23]A. Petosa, *Dielectric Resonator Antenna Handbook* (Artech House Publishers, 2007).
[24]K. El-Mostafa, Y. E. Kharrassi, A. Badreddine, P. Andreoletti, J. Vamecq, M.' Hammed, S. E. Kebbaj, N. Latruffe, G. Lizard, B. Nasser, and M. Cherkaoui-Malki, Molecules **19**, 14879 (2014).
[25]A. Scalisi, B. Morandi, P. Inglese, and R. Lo Bianco, Environ. Exp. Bot. **122**, 158 (2016).
[26]S. Nelson, J. W. Forbus, and K. Lawrence, J. Microwave Power and Electromagnetic Energy **29**(2), 81–93 (2005).
[27]E. Ferro and F. Potortì, IEEE Wirel. Commun. **12**, 12–26 (2005).
[28]S. Banerji and R. S. Chowdhury, Int. J. Mobile Networks Commun. Telematics **3**, 45 (2013).
[29]P. Kumar, S. Dwari, Utkarsh, J. Kumar, and J. Microwaves, Optoelectron. Electromagn. Appl. **16**, 867 (2017).
[30]T. K. Kataria, J. L. Olvera-Cervantes, A. Corona-Chávez, R. Rojas-Laguna, and M. E. Sosa-Morales, Int. J. Food Prop. **20**, 2944 (2017).
[31]D. S. Filonov, E. I. Kretov, S. A. Kurdjumov, V. A. Ivanov, and P. Ginzburg, J. Quant. Spectrosc. Radiat. Transfer **235**, 127 (2019).
[32]S. O. Nelson, *Dielectric Properties of Selected Food Materials Dielectric Properties of Agricultural Materials and their Applications* (Academic Press, 2015), pp. 147–165.
[33]T. P. Marsland and S. Evans, IEE Proc., Part H **134**, 341 (1987).
[34]R. Alaee, C. Rockstuhl, and I. Fernandez-Corbaton, Opt. Commun. **407**, 17 (2018).